

Dynamics of the Reaction $O(^3P) + H_2S \rightarrow OH + SH$. 1. Rotational, Λ Doublet, and Fine Structure Distributions in the $OH(v'' = 1)$ Product

Matthew L. Costen,[†] Gus Hancock,* and Grant A. D. Ritchie

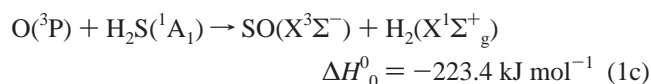
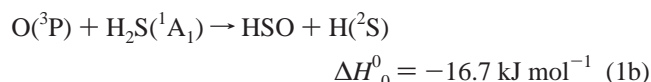
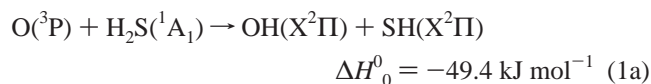
Physical and Theoretical Chemistry Laboratory, Oxford University, South Parks Rd, Oxford, OX1 3QZ, U.K.

Received: June 16, 1999; In Final Form: August 23, 1999

Rotational, spin-orbit, and Λ doublet populations have been measured in the $OH(v'' = 1)$ product of the $O(^3P) + H_2S$ reaction. Ground-state O atoms with kinetic energies above the barrier to reaction were formed by photolysis of NO_2 at 355 nm. Rotational populations were found to be hotter than statistically predicted, with excitation up to the energetic limit in a distribution that suggests efficient conversion of reagent kinetic energy into OH product rotation. Spin-orbit ratios show approximately equal populations in the $^2\Pi_{3/2}$ and $^2\Pi_{1/2}$ states of OH, but Λ doublets favor the symmetric A' level for all measured values of N'' . A model of the dynamics involving a planar transition state is invoked to explain the observations and predicts the SH cofragment to be formed in the $A'' \Lambda$ doublet with little rotational energy.

I. Introduction

The reaction of oxygen atoms with hydrogen sulfide is a prototype for sulfur oxidation in the atmosphere and a major source of sulfates from the combustion of sulfur-contaminated fossil fuels. The reaction can occur via three competing pathways,¹



The kinetics of the reaction have been extensively studied by a number of techniques. The products have been detected by photoionization mass spectroscopy,² electron spin resonance,³ and atomic resonance spectroscopy with discharge flow⁴ and flash photolysis initiation.⁵ The slow rate constant at room temperature, $2.2 \times 10^{-14} \text{ cm}^3 \text{ molecule}^{-1} \text{ s}^{-1}$, indicates the presence of a barrier, and the activation energy has been determined⁶ to be 16 kJ mol^{-1} . Channels 1a and 1b have both been observed, but despite attempts to detect the SO product by mass spectroscopy channel 1c has never been reported. The branching ratio for the two observed channels has been recommended to be $k_{1a}/(k_{1a} + k_{1b}) > 0.8$.⁷

The dynamics of reaction 1b have been studied in crossed molecular beam experiments by two groups, by Grice et al.⁸ at a collision energy of 30.1 kJ mol^{-1} and at higher resolution by Casavecchia et al.⁹ at collision energies of 32.1 and 49.4 kJ mol^{-1} . Grice et al. found a near isotropic scattering distribution with almost all the available energy released into translation,

with a threshold energy for the reaction of $14.2 \pm 2.1 \text{ kJ mol}^{-1}$, equal, within experimental error, to the measured activation energy. Casavecchia et al. report the HSO product to be scattered almost entirely into the backward hemisphere, with approximately 60% of the available energy being released into translation of the products. This has been interpreted by a model featuring attack by the electrophilic $O(^3P)$ atom on the sulfur out-of-plane lone pair, the highest occupied molecular orbital, to form a pyramidal intermediate. This then relaxes through a planar transition state before dissociating, consistent with recent ab initio calculations.¹⁰

The assumed major channel, (channel 1a), has by contrast received relatively little attention. The $v'' = 0$ to $v'' = 1$ vibrational branching ratio has been measured to be 0.45:0.55 by laser-induced fluorescence (LIF) on the rotationally relaxed OH product with the $O(^3P)$ produced by microwave discharge.¹¹ No previous measurements have been reported of the rotational distributions or fine structure ratios.

In this and the following paper we report an extensive investigation into the reaction dynamics of channel 1a through laser-induced fluorescence (LIF) measurements of the nascent OH fragment. $O(^3P)$ atoms are formed from the 355 nm photolysis of NO_2 with translational energies such that some 40% of their collisions with thermal H_2S occur with relative kinetic energies above the measured activation energy. In this paper (part 1) we report on the *scalar* properties of the OH fragment, namely, the rotational, fine structure, and Λ doublet populations of the dominant OH vibrational level, $v'' = 1$. For $OH(v'' = 0)$ we report the strong interference from the photolysis product of HONO, an unavoidable contaminant under our experimental conditions. We produce $O(^3P)$ atoms with aligned velocities, and in the following paper (part 2)¹² we report measurements of the *vector* attributes of the reaction, namely, the alignment of the $OH(v = 0, 1)$ product velocity and angular momentum vectors relative to the initial velocity vector of the reagents.

II. Rotational Distributions from LIF

A number of different factors can influence the intensity of a transition in LIF, and careful consideration of their contribu-

* To whom correspondence should be addressed. E-mail: gus.hancock@chemistry.ox.ac.uk. Fax: (+44) 1865 275410.

[†] Current address: Chemistry Department, Brookhaven National Laboratory, Upton, NY 11973-5000.

tions is necessary if accurate populations are to be determined. The populations given in this paper are relative rotational distributions within a single vibrational level. The absolute oscillator strength is thus not relevant, and the assumption is also made that the Franck–Condon factor is constant across the vibrational band studied. The efficiency of the collection optics and any filters used across the emission band must also be ascertained, and the quantum efficiency of the photomultiplier tube (PMT) used can be considered to be constant across the small emission range in these experiments. Within these approximations the intensity of the rotational transition depends, as shown by Greene and Zare,¹³ on the population, rotational line strengths, and laboratory (LAB) frame quadrupole rotational alignment of the product. The general expression for the intensity, I , of a $1 + 1$ LIF transition is then

$$I \propto \frac{S_{J_i} N_{J_i} F(J_i, J_e, J_f)}{g_{J_i}} \quad (2)$$

where S_{J_i} is the transition line strength for the excitation step, g_{J_i} is the degeneracy of the initial state $|v_i, J_i\rangle$, which has population N_{J_i} . The final term $F(J_i, J_e, J_f)$ contains the information on the LAB frame rotational alignment of the product. This is dependent both on the nature of the transition via the angular momentum coupling factors linking the initial, excited, and final states and on the relative geometry of the photolysis, probe, and detection propagation directions and electric vectors. The alignment term has the form

$$F(J_i, J_e, J_f) = b_0 + \frac{5}{4} b_1 A_0^{(2)}(\text{LAB}) \quad (3)$$

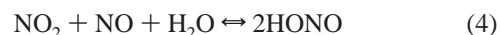
where $A_0^{(2)}(\text{LAB})$ is the laboratory frame quadrupole rotational alignment having limits between $-2/5$ and $+4/5$, and b_0 and b_1 are the angular momentum and geometrical factors. The spectroscopy of OH results in multiple emission branches for each excitation step, and these are not resolved in this experiment. The $F(J_i, J_e, J_f)$ term must thus be weighted over the emission steps according to the line strengths and relevant filter transmissions. The alignment term can be measured by recording the relative intensity of a transition at two experimental geometries as discussed below.

III. Experimental Section

Experiments were performed in a hexagonal stainless steel vacuum chamber equipped with a variety of baffle arms and ports and pumped by an oil diffusion pump capable of sustaining a base pressure of 1×10^{-6} Torr. The reagents, H₂S (Cambrian Gases, 99.8%) and NO₂ (BOC, 99.5%), were stored prior to and during experiments in a glass vacuum line and were both freeze/thaw purified at liquid nitrogen temperatures before use. The pressure in the reaction chamber was maintained at 100 mTorr in a 50:50 mixture by varying the flow rates of the reagents and throttling the diffusion pump via a gate valve. The reaction was initiated by the photolysis of NO₂ by 355 nm radiation from the third harmonic of a Nd:YAG laser (JK2000) with a typical fluence of 100 mJ cm^{-2} , producing translationally hot O(³P). The polarization of the photolysis laser was initially horizontal in the LAB frame. The beam passed through a KD*P crystal, and application of a potential difference of 3.2 kV across this crystal resulted in the rotation of the plane of polarization to vertical in the LAB frame. This enabled the acquisition of spectra recorded at two different experimental geometries under otherwise identical conditions, and we refer to these as

geometries A (photolysis laser vertically polarized) and B (photolysis laser horizontally polarized), after Docker.¹⁴ After a delay of 200 ns the product OH(X²Π) was probed generally via the A²Σ⁺–X²Π (0,1) band around 340 nm using the second harmonic of a Nd:YAG pumped dye laser (Spectron SL803 pumping a modified Spectron SL4000 using LDS698 in methanol with the output frequency doubled in a KD*P crystal). The probe laser fluence was $<500 \mu\text{J cm}^{-2}$, and the signal was found to be linear in probe laser fluence up to this limit, indicating that saturation was not occurring. The probe laser was counterpropagated to the photolysis laser and was vertically polarized in the laboratory frame. The fluorescence was collected perpendicular to the laser axis by an $f/3$ lens and passed through two custom interference filters (Glen-Spectra, 80% transmittance at 240–330 nm, OD > 2 at 340–400 nm, and Laser Components GmbH, $>30\%$ transmittance at 300–320 nm, OD > 3 elsewhere) to discriminate against scattered photolysis and probe light before being imaged onto a photomultiplier tube (EMI 9813QKB). The signals from the photomultiplier and photodiodes monitoring the laser energies were passed to a digital storage oscilloscope (LeCroy 9304, 175 MHz, 100 Msamples s^{-1}) interfaced to a PC (Dan 486DX33) via the GPIB protocol. This computer also controlled the probe laser wavelength stepping. The PMT signal was normalized to the photolysis and probe laser fluences in a shot-to-shot fashion, with shots having fluence below a preset threshold being rejected. Typically, 30–40 shots were averaged at each wavelength before the probe laser wavelength was incremented by 0.0005 nm, a typical scan consisting of 1000 points. The probe laser wavelength in the fundamental was measured at the start and finish of each scan, and during the scan a portion of the probe laser fundamental output was split off and expanded through a monitor etalon (free spectral range of 0.524 cm^{-1}). The resulting fringe pattern was imaged onto a pinhole photodiode and the output also passed to the oscilloscope. The resulting oscillating signal was subsequently used to ensure that the wavelength scale of each scan was linear in frequency.

Previous studies of reactions producing OH using NO₂ photolysis as an O(³P) source have been hindered by the production of OH by the photolysis of contaminant HONO.^{15,16} NO₂ and H₂S react slowly in the gas phase ($k < 6 \times 10^{-20} \text{ cm}^3 \text{ molecule}^{-1} \text{ s}^{-1}$)¹⁷ but may react faster on surfaces, and as a first precaution, the reagents were not premixed. The 355 nm photolysis of HONO produces vibrationally and rotationally cold OH, predominately in the $v'' = 0$, $N'' \leq 6$ states. OH produced promptly in these states, indicative of a photodissociation process, was observed with only NO₂ present. HONO exists in equilibrium with NO, H₂O, and NO₂:



The NO impurity may be removed by the three-body recombination reaction



Samples of NO₂ were thus left overnight with excess O₂, frozen with a diacetone alcohol/dry ice slush at 218 K and pumped to remove residual NO and O₂. This greatly reduced the HONO contribution to the OH signal, although it could not be eliminated. No OH product was found in $v'' = 1$ states from the photolysis of NO₂ alone, even under conditions in which very large signals were observed in $v'' = 0$. This is consistent with the observations of McKendrick et al.¹⁶

The addition of H₂S resulted in an OH signal in $v'' = 1$, which increased with delay between the photolysis and probe

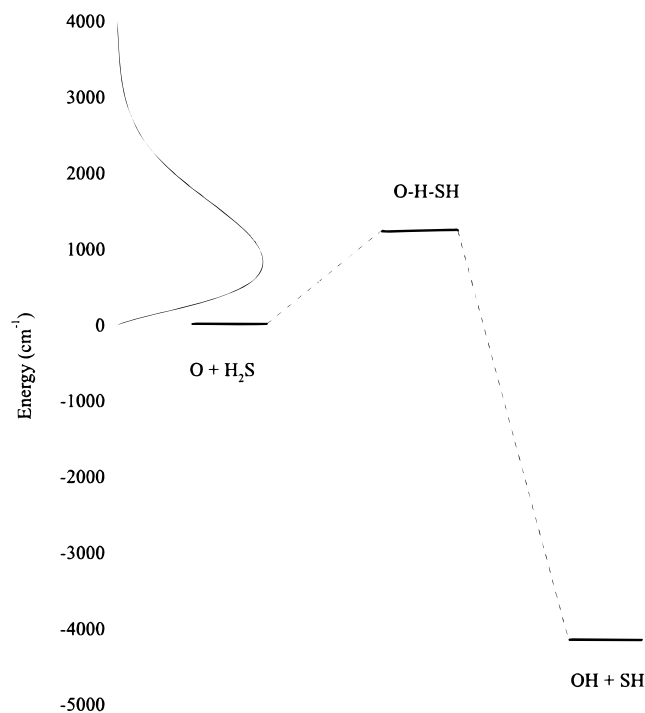


Figure 1. Energy level diagram for the reaction $\text{O} + \text{H}_2\text{S} \rightarrow \text{OH} + \text{SH}$. The barrier to reaction is taken from activation energy measurements, and the kinetic energy distribution of the reagents is calculated from eq 6.

lasers and was linear in the photolysis laser fluence, indicative of a reactive process. A similar signal was also found in the $v'' = 0$, $6 < N'' < 12$ states, but this was found to require NO_2 only and to display a greater than linear dependence on the fluence of the photolysis laser. This signal is thought to arise from energy transfer between OH produced from contaminant HONO photolysis and rotationally excited NO from the 355 nm NO_2 photolysis. The limit of OH production by this method, $N'' \leq 12$, corresponds well to the maximum energy available in the NO produced by photolysis ($\sim 3000 \text{ cm}^{-1}$). Even with extensive purification of the NO_2 before use these contaminant signals restricted the observation of OH product from the reaction of $\text{O}(\text{}^3\text{P})$ and H_2S to $v'' = 0$, $N'' > 12$, and $v'' = 1$.

The rotational distribution of the product of a reaction will only contain significant information if it is free from collisional effects after formation, i.e., if it is nascent. Similarly, in a reaction involving a translationally hot atom such as $\text{O}(\text{}^3\text{P})$ from NO_2 photolysis the initial collision velocity distribution must be preserved. An upper limit for the collision frequency for the fastest moving species in the system, $\text{O}(\text{}^3\text{P})$, can be estimated from the hard-sphere collision rate for the largest of the target species. The resulting collision frequency can then be used to calculate a product of the total pressure and time delay, $p\Delta t$, at which, on average, one collision would be expected to occur. The result for this system is found to be $3.7 \times 10^{-8} \text{ Torr s}$. This may be compared to $4 \times 10^{-8} \text{ Torr s}$ calculated for the similar $\text{O}(\text{}^3\text{P}) + \text{HBr}$ system.¹⁶ The collision rate may then be modeled as a Poisson distribution. The experiments reported here were all performed with $p\Delta t \leq 2 \times 10^{-8} \text{ Torr s}$, resulting in less than 12.5% of the fastest $\text{O}(\text{}^3\text{P})$ produced undergoing a secondary collision. The results presented are thus believed to be due to the reaction of nascent $\text{O}(\text{}^3\text{P})$ and the product OH likewise to be free from secondary collisional effects.

The photolysis of NO_2 at 355 nm produces translationally hot $\text{O}(\text{}^3\text{P})$ atoms, with a range of speeds resulting from the internal energy of the cofragment NO. The target H_2S and parent

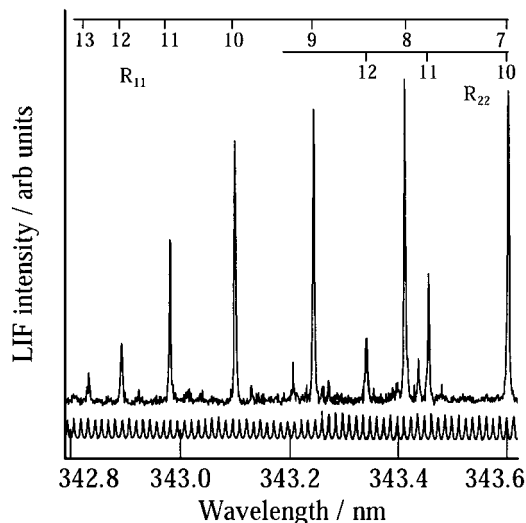


Figure 2. Part of the (0, 1) band of the OH ($\text{A}^2\Sigma^+ - \text{X}^2\Pi$) system recorded from the nascent products of the $\text{O} + \text{H}_2\text{S}$ reaction. Transitions from specific N'' levels in the R_{11} and R_{22} bands are shown, together with the monitor etalon fringes.

NO_2 also have Maxwell–Boltzmann velocity distributions that further broaden the collisional energy distribution. The effect of these precursor and target velocity distributions on the relative collision velocity of a photon-initiated reaction has been considered by several authors.^{18,19} For a monoenergetic hot atom the result can be resolved into speed and angular components of which the speed distribution, $A(k)$, is given by

$$A(k) = \left(\frac{1}{2\omega^2} \right) \left(\frac{k^3}{u_A} \right)^{1/2} \exp \left[- \frac{(u_A^2 + k^2)}{2\omega^2} \right] I_{1/2} \left(\frac{u_A k}{\omega^2} \right) \quad (6)$$

where k is the collision speed, u_A is the hot atom speed, and $\omega^2 = [k_B T(m_{AD} + m_{BC}) / (m_{AD} m_{BC})]$, with AD the precursor and BC the target. $I_{1/2}$ is a modified spherical Bessel function.¹⁹ The $\text{O}(\text{}^3\text{P})$ speed distribution from the photolysis can be well represented²⁰ by two equally weighted Gaussians with centers at 980 and 1600 ms^{-1} and standard deviations of 200 ms^{-1} . The overall collisional energy distribution can then be found by numerically integrating eq 6 over the Gaussians using Monte Carlo selection. Figure 1 shows the resultant energy distribution relative to the thermodynamics of process 1a.

IV. Results

Relative rotational population distributions for the $v'' = 1$ level of the OH product of the reaction of $\text{O}(\text{}^3\text{P})$ with H_2S were extracted from multiple scans over the (0, 1) band of the OH- ($\text{A}^2\Sigma^+ - \text{X}^2\Pi$) transition. Spectra were recorded in scans over typically 1 nm at a time with a step size of 0.0005 nm to ensure an adequate number of points across a rotational transition, and an example including transitions in the R_{11} and R_{22} band regions is shown in Figure 2. The integral areas of transitions that were not significantly overlapped by neighboring lines were then found from Gaussian fits. The intensity of a transition will depend, as shown in eqs 2 and 3, on the LAB frame rotational angular momentum alignment as well as the population. A variety of transitions were recorded using the KD*P crystal to switch the experimental geometry between those defined as A and B, and an example scan for transitions pumped on the (1, 1) band near 315 nm is shown in Figure 3. It was found that any change in the measured intensity due to the LAB frame alignment was smaller than the statistical variation of the line

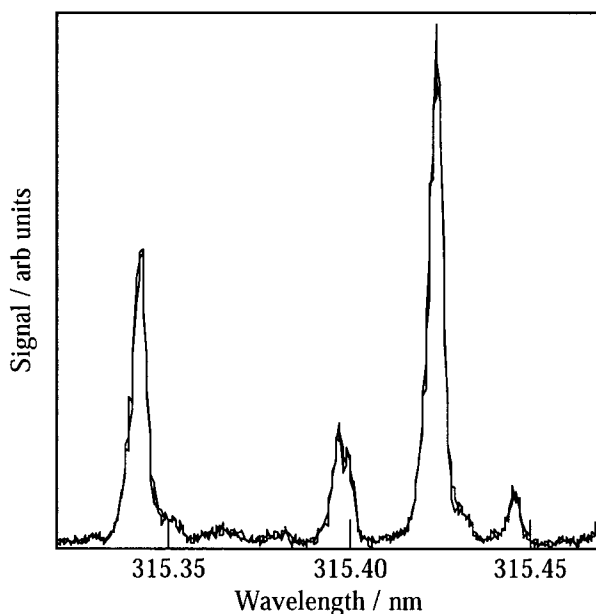


Figure 3. Part of the (1, 1) band of the OH ($A^2\Sigma^+ - X^2\Pi$) system recorded from the nascent products of the O + H₂S reaction, with orthogonal polarizations of the photolysis laser (Docker geometries A and B).¹⁴ The invariance of the two signals within experimental error allows rotational populations to be extracted without correction for polarization dependence of the LIF process.

intensity. The quoted populations have thus been calculated on the basis of no LAB frame rotational alignment of the product. In the following paper¹² we consider more detailed measurements of the LAB frame alignment at higher resolution, in which we find a maximum difference of 5% between the signals measured for geometries A and B. This leads to a rotational alignment correction of at most 5% in the populations and will not affect the conclusions drawn in this study.

Figure 4 shows the rotational distributions for $v'' = 1$ for the F₁ and F₂ spin-orbit manifolds ($^2\Pi_{3/2}$ and $^2\Pi_{1/2}$, respectively) and the A' and A'' Λ doublet levels as a function of rotational quantum number N'' . The rotational distributions all show a similar general form, rising to a peak at $N'' = 7$ before falling sharply to zero at $N'' = 13$. The Λ doublet ratios for the two spin-orbit manifolds are shown in Figure 5a, and a clear preference for the A' over the A'' doublet is seen, which is independent of either spin-orbit manifold or rotational quantum number. Finally, the spin-orbit ratio as a function of N'' is shown in Figure 5b, corrected for the appropriate ratio of degeneracies of the rotational levels. Although there is a slight preference for the lower spin-orbit state of OH($^2\Pi_{3/2}$) at high values of N'' , the data are sufficiently scattered around zero to suggest that there is no significant dynamical bias toward either state.

V. Discussion

The amount of information contained in the rotational distributions measured may be determined by the application of information theory to the results in the form of a surprisal plot.²¹ The surprisal requires a model distribution with which to compare the experimental results, and the simplest and most entropic distribution is the prior, in which all states energetically accessible are populated according to their degeneracies subject only to normalization and energy conservation. The probability of populating an OH vibrational v , rotational N , spin-orbit Ω , and Λ doublet state A according to these constraints is given by the expression

$$P(v, N, \Omega, A; E_{\text{tot}}) = \frac{(2J_{\text{OH}} + 1) \sum_{\nu_{\text{SH}}} \sum_{J_{\text{SH}}} \sum_{\Omega_{\text{SH}}} \sum_{A_{\text{SH}}} (2J_{\text{SH}} + 1) (E_{\text{tot}} - E_{\text{OH}} - E_{\text{SH}})^{1/2}}{Q} \quad (7)$$

where A is the Λ doublet level, Q is the total sum over all accessible levels, and E_{tot} is the total available energy. The calculation was performed using the OH state energies given by Diecke and Crosswhite²² and those for SH calculated from the data of Huber and Herzberg.²³ The total available energy depends on the collisional energy distribution as well as the exothermicity, and the rotational probability distributions were numerically integrated over the collisional energy distribution shown in Figure 1. The surprisal $I(R)$ is then given by

$$I(R) = -\ln \left[\frac{P(R)}{P^0(R)} \right] \quad (8)$$

where $P(R)$ is the experimental distribution and $P^0(R)$ the prior for a rotational quantum state R . The resulting surprisals plotted against the fraction of the available energy appearing as rotation, $g(R)$, for the four spin-orbit and Λ doublet manifolds of OH- ($v'' = 1$) are shown in Figure 6. The surprisal plots are seen to be close to linear, with negative gradients indicating that the rotational distributions are hotter than the prior, and the slopes are the same, within experimental error, for both Λ doublets and spin-orbit states. The nonstatistical nature of the surprisal plot suggests that a complex-forming mechanism is not the primary reaction path. The next most entropic model distribution would be phase space theory (PST), the calculation of which requires a knowledge of the (unknown) opacity function for the reaction. The transfer of a light atom between two heavier atoms will result in high pre- and postcollision orbital angular momenta, and this together with the low total angular momenta possible in the OH and SH because of their large rotational energy spacings suggests that there will not be any strong angular momentum conservation constraints present, and PST will thus be expected to be similar to the prior.

The limit of the observed rotational population, at $N'' = 13$, is very close to the energetic limit formed by the exothermicity and maximum collision energy. The rotational distributions may be plotted together with the available energy distribution formed by the sum of the exothermicity and collisional energy distribution, and this is shown in Figure 7 for each of the four spin-orbit and Λ doublet distributions scaled so that the sum of their populations are the same. The falloff in the rotational distributions lie on this kinetic energy distribution within their errors, suggesting that these high rotational states are formed in coincidence with SH with virtually no internal energy. This very efficient mapping of the available energy into rotation of the newly formed diatomic product suggests a direct mechanism through bent transition states. A similar efficient conversion of translational energy into product rotation has also been observed in the reaction of hot O(3P) atoms with CS($X^1\Sigma^+$)²⁰ and is presently being tested in the O + H₂S reaction by measurements of the nascent rotational distributions in OH for differing O atom translational energies.

The Λ doublets are defined such that the levels which in the high J limit have a wave function that is symmetric with respect to the reflection of the spatial coordinates of the electrons in the plane of rotation are labeled A', and those that are antisymmetric with respect to the same reflection are labeled A''.²⁴ The chemical significance of Λ doublet ratios has been

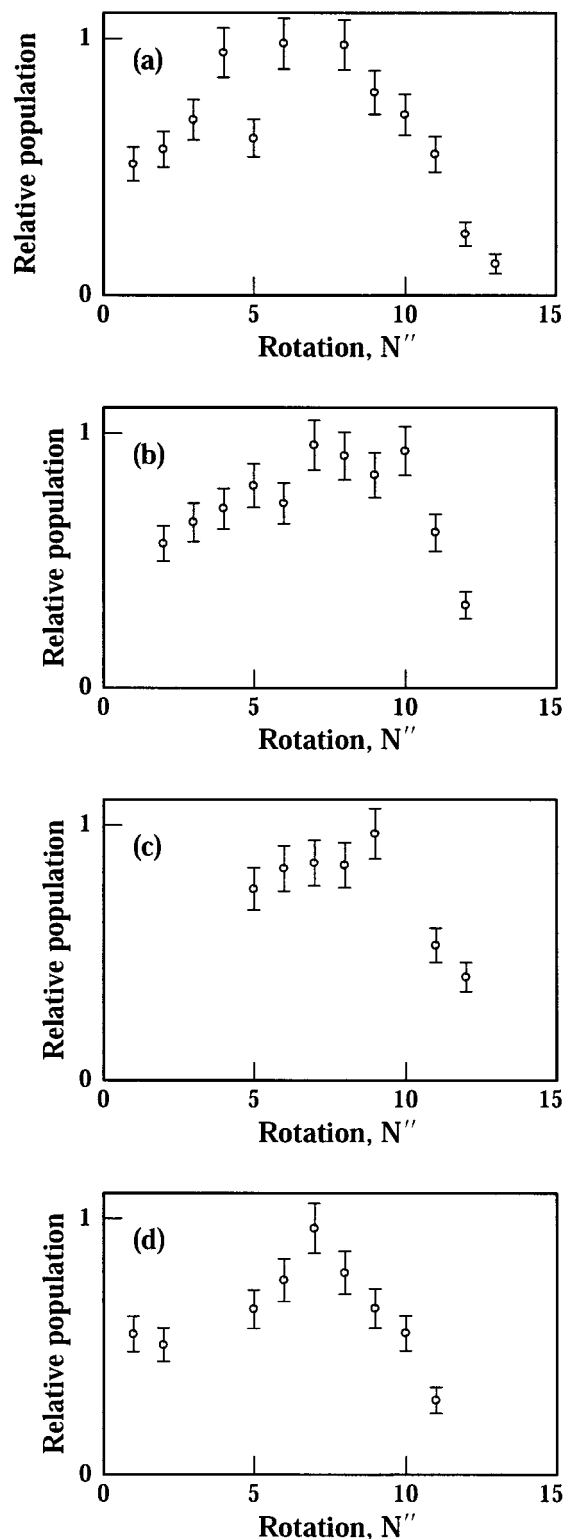


Figure 4. Relative populations of the four subsets of OH rotational levels in $v'' = 1$ as a function of rotational quantum number N'' : (a) ${}^2\Pi_{3/2}$ (A'), (b) ${}^2\Pi_{3/2}$ (A''), (c) ${}^2\Pi_{1/2}$ (A'), and (d) ${}^2\Pi_{1/2}$ (A'') where A' and A'' refer to the symmetries of the OH Λ doublets. Distributions are arbitrarily scaled, and all show the same approximate form, peaking at $N'' \approx 7$ and falling to the energetically allowed limit at $N'' = 13$. Error bars show 2σ standard deviations from multiple measurements.

discussed by Andresen and Rothe.²⁵ In the limit of high nuclear rotation the Λ doublets can be identified with the symmetry with respect to reflection in the plane of rotation of the electronic wave function, but at lower N'' the degree of electron alignment decreases, reducing the maximum population ratio that can be

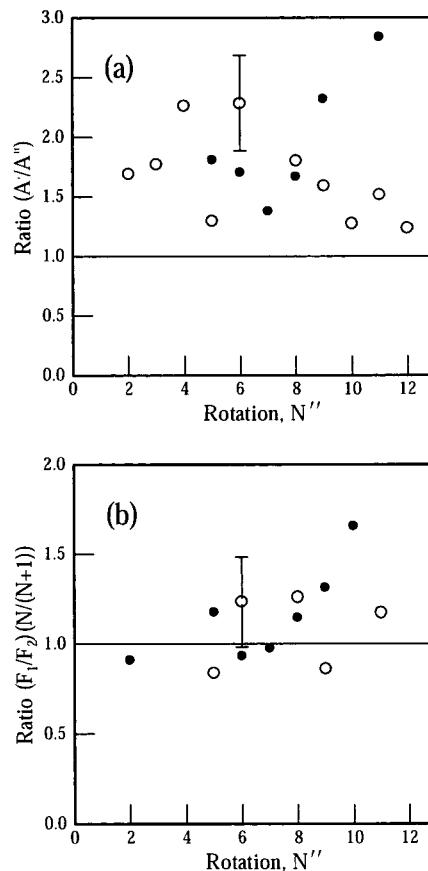


Figure 5. Λ doublet ratios (a, open circles F_1 , filled circles F_2) and spin-orbit ratios (b, open circles A' , filled circles A'') for the OH($v = 1$) product of reaction 1a taken from the data of Figure 4. A preference for the A' symmetric Λ doublet is seen for both spin-orbit states, while no clear preference for either spin-orbit manifold is seen.

measured. Any measured Λ doublet ratio must thus be considered in the light of the maximum ratio possible. The degree of electron alignment increases rapidly with N'' for OH, the Λ doublets are well defined, and in principle high ratios are possible, as seen for example in the photodissociation of jet-cooled H_2O .²⁶ In the present case we see a clear preference for the A' Λ doublet over the A'' (Figure 5a), which in the high rotation limit means that the half-filled Π orbital on OH lies preferentially in the plane of rotation. We first consider a statistical model for Λ doublet ratios, which predicts that under certain conditions the ratio of A'/A'' population should equal 2 and is based on a random distribution of dissociation geometries leading preferentially to twice as many A' as A'' final states.²⁷ The model has successfully predicted the outcome of a number of H atom reactions forming OH but relies on the plane of rotation of the OH product being defined by the velocity of the attacking atomic reagent (the H atom). When the attacking atom is light, then the force on the OH fragment is largely directed at its center of mass and gives a low torque and thus contributes little to the product angular momentum. For the present case, however, a heavy atom is the attacker and a light atom is transferred, and in addition the transition state is formed via a barrier in which the kinetic energy of the O atom is converted into potential energy of the system. Both effects mean that the velocity of the O atom does not determine the OH plane of rotation (the product angular momentum comes largely from the impulse on the light H atom) and means that the model is not applicable. We consider instead a model of the reaction

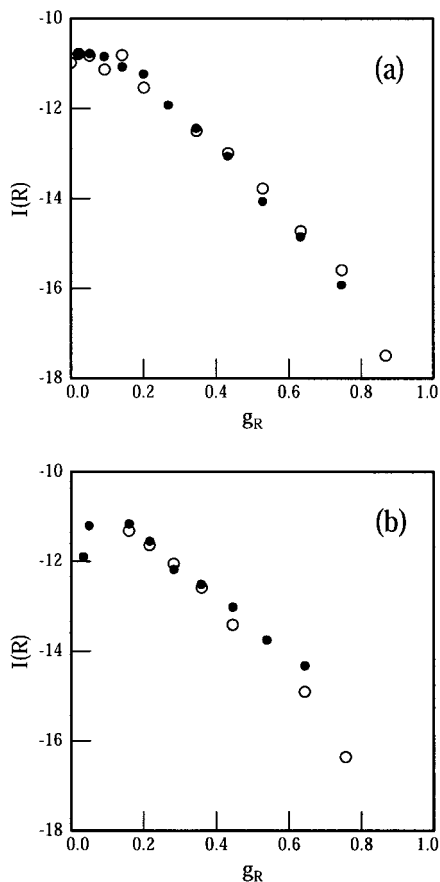


Figure 6. Surprisal plots $I(R)$ for (a) $F_1(^2\Pi_{3/2})$ and (b) $F_2(^2\Pi_{1/2})$ for the OH($v'' = 1$) product of reaction 1a as a function of $g(R)$, the fraction of available energy present as rotation. For each spin-orbit state the Λ doublets are plotted and analyzed separately (open circles A' , filled circles A'') and show slopes that are the same within experimental error and whose negative values indicate a higher than statistical fraction of available energy appearing in rotation of OH($v'' = 1$).

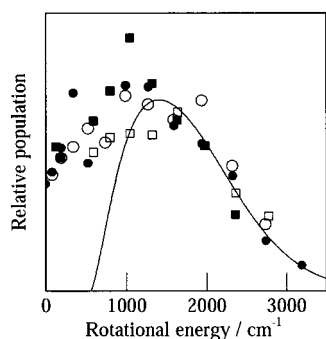


Figure 7. Populations of the four sets of levels of OH($v'' = 1$) produced in the O + H₂S reaction as a function of their rotational energy and compared with the distribution of available energy in the reaction. The filled circles correspond to the F_1A' Λ doublet, the open circles to F_1A'' , the open squares to F_2A' , and the filled squares to the F_2A'' . Each of the four distributions has been scaled so that the sum of the level populations is unity. The available energy is defined as the exothermicity of the reaction forming OH($v'' = 1$) plus the relative collisional energy distribution defined by eq 6. The similarity between the high rotational energy distributions and the falloff of the relative kinetic energy function suggests efficient conversion of high reagent translational energy into OH rotation.

pathway that conserves planarity through the transition state and that can lead to unequal Λ doublet ratios.

The ab initio transition state calculated by Goumri et al.¹⁰ for the reaction path leading to OH + SH is planar and of A''

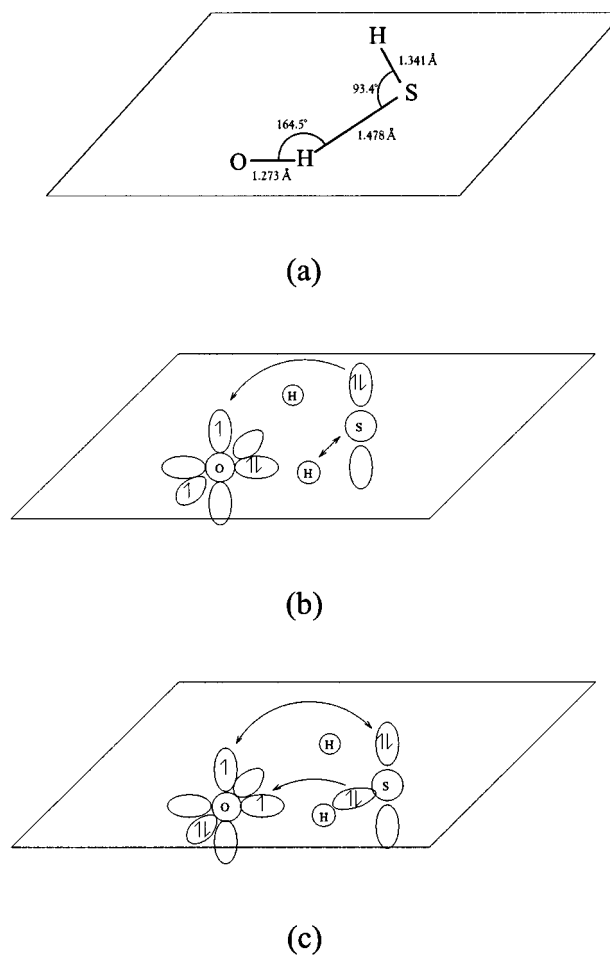


Figure 8. (a) Planar transition state for the O + H₂S \rightarrow OH + SH reaction from ref 10. (b, c) Two possible mechanisms for the attack of O atoms on H₂S are illustrated, with the single-ended arrows showing the electron transfers. Both mechanisms predict the OH and SH products to have opposite Λ doublet propensities, with mechanism b predicting OH in the A' state (as experimentally observed) and mechanism c predicting OH in the A'' state.

symmetry, and this is shown in Figure 8a. We take this as the starting point for two simple molecular orbital models of the O atom approach to the H₂S. The first model has the O(³P) attacking the H atom with its filled p orbital, with transfer of a H atom to form the OH bond, leaving electron density in the lowest unoccupied molecular orbital (LUMO) on H₂S, which has a_1 symmetry and is antibonding, thus initiating repulsion between the S and H atoms (Figure 8b). The highest occupied molecular orbital (HOMO) of H₂S has b_1 symmetry and represents a mostly nonbonding orbital localized on the sulfur atom and perpendicular to the plane. The transition state can be stabilized by the overlap of this HOMO with one of the partially filled p orbitals of the oxygen atom that lies perpendicular to the reaction plane, and transfer of an electron out of the HOMO into this results in it evolving into a filled orbital of OH (largely a nonbonding orbital located on the O atom). The other half-filled orbital remains in the plane and becomes the half-filled p Π orbital resulting in the A' Λ doublet in OH. The HOMO on the H₂S has meanwhile evolved into the half-filled p Π orbital on SH, indicating a preference for the A'' orbital to be preferentially populated in SH. This model is consistent with the ab initio transition-state symmetry and produces the observed preference for the A' OH Λ doublet.

A second approach geometry, which would also be consistent with the A'' symmetry of the transition state, is when the O(³P)

approaches the H₂S with one of the half-filled p orbitals directed toward the H atom and the other perpendicular to the plane (Figure 8c). Again, the HOMO of the H₂S could stabilize the transition state through overlap with this orbital, but reaction would now require only the transfer of electron density from the SH bonding orbital of H₂S in the plane. This would lead to the half-filled out-of-plane p orbital on the oxygen atom becoming the Λ doublet defining p Π orbital, resulting in a preference for A'' symmetry in OH. The SH Λ doublet would be defined by the half-filled orbital left from the broken SH bond, yielding a SH Λ doublet ratio favoring the A' doublet. This model thus predicts the opposite Λ doublet preference for the OH compared to that which is observed. In either model the Λ doublet ratio would be reduced by a lack of planarity in the transition state caused, for example, by out-of-plane rotation of the H₂S during reaction.

Attempts were made to observe the SH cofragment of the reaction by LIF, but rapid predissociation of the A² Σ^+ upper state and consequent reduction of the fluorescence quantum yield made signals unobservable. The observations of a higher than statistical proportion of the available energy in OH($v = 1$) rotation suggest a low overall rotational excitation in SH, and further details of the scattering discussed in the following paper (part 2)¹² support this prediction. Models for the Λ doublet ratios of the two X² Π reaction products suggest that the fragments will have opposite symmetries, and the observation of a preference for the A' Λ doublet in OH would predict that SH will be formed in the A'' state. Such a prediction can be tested on the SD product of the O + D₂S reaction (predissociation lifetimes for the SD A² Σ^+ state are much longer than those for SH²⁷), and such experiments are planned in our laboratory.

VI. Conclusions

The quantum states produced in OH($v'' = 1$) from the reaction of ground-state thermally hot O(³P) atoms with H₂S show rotational excitation up to the energetic limit with a fraction of the available energy higher than that predicated statistically. The distribution of the highest rotational states reflects the kinetic energy of the reagents and suggests an efficient mapping of translational into rotational energy of the new bond, predicting little excitation of the SH cofragment. Λ doublet ratios favor the formation of A' OH, with the half-filled p Π orbital in the plane of rotation, and a model of the dynamics predicts the opposite Λ doublet in the SH coproduct.

Acknowledgment. We are grateful to the EPSRC for support of this work through the provision of studentships (M.L.C. and G.A.D.R.).

References and Notes

- (1) Balucani, N.; Beneventi, L.; Casavecchia, P.; Stranges, D.; Volpi, G. G. *J. Chem. Phys.* **1991**, *94*, 8611.
- (2) Slagle, I. R.; Baiocchi, F.; Gutman, G. *J. Chem. Phys.* **1978**, *82*, 1333.
- (3) Cupitt, L. T.; Glass, G. P. *J. Chem. Soc., Faraday Trans. 2* **1970**, *65*, 3007.
- (4) Whytock, D. A.; Timmons, R. B.; Lee, J. H.; Michael, J. V.; Payne, W. A.; Steif, L. J. *J. Chem. Phys.* **1976**, *65*, 2052.
- (5) Tsuchiya, K.; Yokohama, K.; Matsui, H.; Oya, M.; Dupre, G. *J. Phys. Chem.* **1994**, *98*, 8419.
- (6) Atkinson, R.; Baulch, D. L.; Cox, R. A.; Hampson, R. F., Jr.; Kerr, J. A.; Troe, J. *J. Phys. Chem. Ref. Data* **1989**, *18*, 881.
- (7) Singleton, D. L.; Cvetanović, R. J. *J. Phys. Chem. Ref. Data* **1988**, *17*, 1377.
- (8) Davidson, F. E.; Clemo, A. R.; Duncan, G. L.; Bowett, R. J.; Dobson, J. H.; Grice, R. *Mol. Phys.* **1982**, *46*, 33.
- (9) Alagi, M.; Balucani, N.; Casavecchia, P.; Stranges, D.; Volpi, G. *J. Chem. Soc., Faraday Trans.* **1995**, *91*, 575.
- (10) Goumri, A.; Laakso, D.; Rocha, J.-D. R.; Smith, C. E.; Marshall, P. *J. Chem. Phys.* **1995**, *102*, 161.
- (11) Agrawaller, B. S.; Setser, D. W. *J. Chem. Phys.* **1987**, *86*, 5421.
- (12) Costen, M. L.; Hancock, G.; Ritchie, G. A. D. *J. Phys. Chem. A* **1999**, *103*, 10651.
- (13) Greene, C. H.; Zare, R. N. *J. Chem. Phys.* **1983**, *78*, 6741.
- (14) Docker, M. P. *J. Chem. Phys.* **1989**, *135*, 405.
- (15) Whitehead, J. C. *Gen. Discuss., Faraday Discuss. Chem. Soc.* **1991**, *91*, 151.
- (16) McKendrick, K. G.; Rakestraw, D. J.; Zare, R. N. *J. Phys. Chem.* **1988**, *92*, 5530.
- (17) Cantrell, C. A.; Davidson, J. A.; Shetter, R. E.; Anderson, B. A.; Calvert, J. G. *J. Phys. Chem.* **1987**, *91*, 6017.
- (18) Gilbert, E. P.; Maitland, G.; Watson, A.; McKendrick, K. G. *J. Chem. Soc., Faraday Trans.* **1993**, *89*, 1527.
- (19) Brouard, M.; Duxon, S.; Enriquez, P. A.; Simons, J. P. *J. Chem. Soc., Faraday Trans.* **1993**, *89*, 1427.
- (20) Costen, M. L.; Hancock, G.; Orr-Ewing, A. J.; Summerfield, D. J. *J. Chem. Phys.* **1994**, *100*, 2754.
- (21) Levine, R. D.; Bernstein, R. B. *Molecular Reaction Dynamics and Chemical Reactivity*; Oxford University Press: Oxford, 1987.
- (22) Dieke, G. H.; Crosswhite, H. M. *J. Quant. Spectrosc. Radiat. Transfer* **1962**, *2*, 97.
- (23) Huber, K. P.; Herzberg, G. *Constants of Diatomic Molecules*; Van Nostrand Reinhold: New York, 1979.
- (24) Alexander, M. H.; Andresen, P.; Bacis, P.; Bersohn, R.; Comes, F. J.; Dagdigian, P. J.; Dixon, R. N.; Field, R. W.; Flynn, G. W.; Gericke, K.-H.; Grant, E. R.; Howard, B. J.; Huber, J. R.; King, D. S.; Kinsey, D. L.; Kleinermanns, K.; Kuchitsu, K.; Luntz, A. C.; McCaffery, A. J.; Pouilly, B.; Reisler, H.; Rosenwaks, S.; Rothe, E. W.; Shapiro, M.; Simons, J. P.; Vasudev, R.; Wiesenfeld, J. R.; Wittig, C.; Zare, R. N. *J. Chem. Phys.* **1988**, *89*, 1749.
- (25) Andresen, P.; Rothe, E. W. *J. Chem. Phys.* **1985**, *82*, 3634.
- (26) Andresen, P.; Ondrey, G. S.; Titze, B.; Rothe, E. W. *J. Chem. Phys.* **1984**, *80*, 2548.
- (27) Bronikowski, M. J.; Zare, R. N. *J. Chem. Phys. Lett.* **1990**, *166*, 5.
- (28) Kawasaki, M.; Sato, H.; Inoue, G.; Suzuki, M. *J. Chem. Phys.* **1989**, *91*, 6758.